Sys Rev Pharm 2021;12(1):1129-1141
A multifaceted review journal in the field of pharmacy

Isolation, Identification and Synthesis of Neolignans from *Phoebe declinata* Leaves: Molecular Modeling and Anticancer Evaluation

Rosmalena Rosmalena[1,3], Vivitri D. Prasasty[2*], Fatmawaty Yazid[3], Emil Budianto[1], Berna Elya[4], Puspa Lotulung[5], Hanita Omar[6], Muhammad Hanafi[5,7*]

[1]Department of Chemistry, Faculty of Mathematics and Natural Sciences, Universitas Indonesia, Depok 16424, Indonesia
[2]Faculty of Biotechnology, Atma Jaya Catholic University of Indonesia, Jakarta 12930, Indonesia
[3]Department of Medical Chemistry, Faculty of Medicine, Universitas Indonesia, Jakarta 10430, Indonesia
[4]Faculty of Pharmacy, Universitas Indonesia, Depok 16424, Indonesia
[5]Research Center for Chemistry, Indonesian Institute of Sciences, South Tangerang, Banten 15314, Indonesia
[6]Centre For Foundation Studies in Science, Chemistry Division, University of Malaya, Kuala Lumpur 50603, Malaysia
[7]Faculty of Pharmacy, University of Pancasila, Jakarta 12640, Indonesia

ABSTRACT

Two series of neolignans, aristoligol (**R1**) and aristoligone (**R2**), had been isolated from *P. declinata* Nees (Lauraceae) plant leaves. Dichloromethane (D.C.M.) was used to isolate **R1** and **R2** using flask silica column chromatography as a stationary phase. Meanwhile, n-hexane, dichloromethane, and methanol were used as mobile phases. Moreover, the synthesis of compound R**2** to produce acetyl aristoligol (**R3**) was also done in this study. Compound R2 was synthesized with a reducing agent in methanol ($NaBH_4$/MeOH) to result in a transition compound, the reduced-aristoligol. The transition compound was acetylated with acetic anhydride and catalyzed by D.M.A.P. to produce compound **R3**. The molecular structure identification of all neolignans and their molecular weights was validated by ^{1}H-NMR, ^{13}C-NMR, 2D-NMR, and LC-MS. Further determination of their structure-activity relationship, including molecular modeling and in vitro antiproliferative activity against MCF-7 breast cancer cell lines, showed that compound **R2** has the best binding affinity towards human estrogen receptor-1 (ΔG = -6.7 kcal/mol, Ki = 1.21 x 10^{-5} M). The ADME properties showed that compound R2 is the best one but still less active compared to the standard cancer drug, doxorubicin (ΔG = -8.1 kcal/mol and Ki = 1.14 x 10^{-6} M). Meanwhile, compound **R1** has the highest activity to inhibit the MCF-7 cell proliferation, with a 25 µg/mL concentration, and the highest cytotoxic activity with IC_{50} was 35 µg/mL.

Keywords: Isolation, lignan, *P. declinata*, synthesis, aristoligone derivatives, molecular modeling, anticancer

Correspondence:
Muhammad Hanafi
Email: hanafi124@yahoo.com
Research Center for Chemistry, Indonesian Institute of Sciences, South Tangerang, Banten 15314, Indonesia; Faculty of Pharmacy, University of Pancasila, Jakarta 12640, Indonesia

Vivitri D. Prasasty
Email: vivitri.dewi@atmajaya.ac.id
Faculty of Biotechnology, Atma Jaya Catholic University of Indonesia, Jakarta 12930, Indonesia

INTRODUCTION

Lignans belong to the phytoestrogens group, which are widely found in the plant kingdom [1]. Their primary functions are plant defenses, such as antimicrobes, antifungi, and insecticides [2]. The genus comprises over than 200 species, distributed in Indonesia, Malaysia, India, West Europe, and South America. The phytochemical studies on the genus have shown various activities such as antitumor, antiplasmodial, antimicrobial, antifungal, antidiabetic, muscle relaxant, and many more [3, 4]. Lignans are classified as nonsteroidal polyphenolic plant metabolites that induce biological responses towards the human estrogen receptor by mimicking or modulating endogenous estrogen action. Because of its bioactivity as an antitumor, plant-rich foods with high phytoestrogens contents have been suggested as the biological rationale for the low breast cancer incidence in women, particularly in Asian populations [5].

The study of phytoestrogen effect on estrogen-induced breast cancers is still limited. The insight into the relationship between phytoestrogens and human mammary carcinogenesis is controversial and contentious debate, make these compounds have become an essential topic of research, including experimental, epidemiological, and prospective studies [6]. Phytoestrogens obtained from flavanoids, isoflavonoids, lignans, coumestans, and stilbenes have shown various bioactivities against breast cancers [7]. Some of them can reduce the risk of breast cancer and other hormone-dependent cancers [8], but some others do not have any effect or even can induce the risk of breast cancer [8, 9].

Lignans from some plant species also show cytotoxic activities. Lignans extracted from *Vitex negundo* possess cytotoxic activity and apoptosis induction towards breast cancer cell line MDA-MB-435 and liver cancer cell line SMMC-7721 [10]. Another type of lignan is aryl naphthalene lignan justicidin B from the hair root of *Linum leonii* has a potent cytotoxic and proapoptotic agent against promyelocytic leukemia cell line HL-60 by inducing the activation of the intrinsic mitochondrial cell-death signaling pathways [11]. Edible lignans from various nuts, seeds, and whole-grain cereals have also been found to have weak estrogen-like activity in some hormone-related cancers. However, the cytotoxic study of lignans isolated from *P. declinata* is very limited and less numerous than other plant sources.

P. declinata is naturally abundant in the Indonesian tropical rainforest [12]. This plant is a long-lived perennial and reaches about 9-10 meters in height [13, 14]. *P. declinata* is locally known in Indonesia as *huruhejo* or *bedagai* and commonly grows in Sumatera and Java islands [13]. Lignans from *P. declinata* this research aimed to isolate lignan substituents from *P. declinata* leaves and evaluate its derivatives in silico. The isolated lignans and their derivatives were purified and elucidated using column chromatography, Liquid Chromatography-Mass Spectroscopy (LC-MS), and ^{1}H-^{13}C N.M.R. Spectroscopy. The lignan derivatives were obtained from organic chemical syntheses by reducing agents in methanolic

solvent and acetylation reactions. Moreover, these lignans were analyzed their Q.S.A.R., including drug-likeness properties and molecular docking towards human estrogen receptor to provide insights on their potential estrogen-like activities in silico.

Even though the bioactivity of natural phytoestrogens relevant to breast cancer risk is still not clear, they have commonly been presumed that some of their health-promoting effects might be modulated through estrogen receptor binding [15, 16]. Moreover, chemical transformation of lignan derivatives such as aristoligone and aristoligol from precursor galbulin and isogalbulin, respectively, with general syn–anti substituents in the tetrahydronaphthalene (T.H.N.) framework and $NaBH_4$ reduction, respectively. [17]. The synthetic aristoligone and aristoligol have demonstrated significant pharmacological activities as antitumor [17, 18]. Here we report neolignans derived from aristoligone with quantitative structure-activity relationship properties from NMR spectroscopy identification, synthesis, molecular modeling, and antiproliferative effect towards MCF-7 cell lines. We believe that our study related to the synthetic neolignans would improve their biological activities to inhibit the human estrogen receptor, which could indicate the cytotoxic effect to cancer cells compared to the parental lignans.

MATERIALS AND METHODS

Chemicals

For extraction, fractionation and purification were used distilled solvents for monitoring of purification. The ^{1}H-NMR and ^{13}C-NMR spectra were recorded in a deuterated solvent like $CDCl_3$, CD_3OD, and D_2O, on an NMR 500 MHz (Jeol). Chemical shifts are reported in ppm scale, and the coupling constants are given in Hz. Silica gel 60, 70-230 mesh ASTM (Merck 7734), and silica gel 60, 230-400 Mesh ASTM (Merck 9385) were used for column and flash chromatography, respectively.

Plant sample preparation

P. declinata Nees leaves were collected from Bogor Botanical Garden, Bogor, West Java, Indonesia. An identified specimen (ID No.:PD 1601) was deposited at the Herbarium of Department of Chemistry, Faculty of Medicine, Universitas Indonesia, Jakarta, Indonesia; and at the Herbarium of the Bogor Botanical Garden, Bogor, West Java, Indonesia.

Isolation of lignan from P. declinata leaves

P. declinata Nees (3.0 kg) were ground and extracted for 12 hours by Soxhlet extraction with hexane, followed by CH_2Cl_2. Extraction of neolignans was carried out by following Kuusipalo et al. and Elya et al. with modifications [12,13] and 43.0 g of dichloromethane crude extract. The crude extract was run in a silica chromatography column using CH_2Cl_2 gradually mixed with methanol to separate the bioactive compounds and yield 130 fractions. These fractions were run on TLC plat and showed 15 fraction profiles. Fractions 8-13 (0.3 g) belonged to two neolignans identified as aristoligol (R1) (PTLC; CH_2Cl_2-MeOH 98:2), then fraction 12 (190 mg) was also separated by preparative TLC over silica plat using CH_2Cl_2 : MeOH (95:5), saturated with NH_4OH. The fraction was separated by chromatography column and preparative thin-layer chromatography (TLC) to obtain aristoligone (R2) as a colorless crystal.

Synthesis of lignan derivatives

Reduction of R2 Compounds (Aristoligone)

About 200 mg Aristoligone (**R2**) compound (MW = 370,18) was reduced using a reducing agent, $NaBH_4$ in methanol solvent (1:4), showed a change in Rf value in TLC, to a smaller (polar) value. It showed that the ketone group had been altered into an alcoholic lignan, reduced-aristoligol (MW = 372) in about 7 hours of reaction. After the reaction process was considered complete, the sample was added with water and extracted successively using hexane and ethyl acetate solvents. Ethyl acetate fraction was selected as the desired product, and after evaporation, the recrystallization process was carried out by saturating the solution in dichloromethane and hexane. The crystal formed was separated and weighed as 205.6 mg (0.5527 mmol, 100%), in the form of colorless crystals.

Esterification (Acetylation) R3 compound (Aristoligol)

In studying the relationship between structure and activity, the 20 mg of reduced-aristoligol (MW = 372,2) compound was synthesized by acetylating the compound using the excess of acetyl anhydride (Ac_2O) (1 mL) with N, N-dimethylamino pyridine (DMAP) catalyst in chloroform ($CHCl_3$) solvent. Within a few hours, there has been a change in Rf value (as greater value) at TLC, so it is strongly assumed that the esterification process has occurred. Through the extraction process using n-hexane, and after evaporation, the results obtained were recrystallized with dichloromethane-hexane and produced 22 mg of colorless crystals of acetyl aristoligol (**R3**) with MW = 414.20, with a yield of around 98%.

Protein and Ligand Structure Preparation Methods

The 3D structure of the hESR-1 protein is obtained from https://www.rcsb.org/structure/1UOM (PDB ID = 1UOM), where deletions were carried out on origin ligand`s bond (2-phenyl-1-[4-(2-piperidine-1-yl-ethoxy)-phenyl]-1,2,3,4-tetrahydroisoquinoline-6-ol) in the protein crystal structure and water molecules using the Chimera 1.8.1 program [19, 20]. The protein structure without the ligand was evaluated by its constituent amino acid coordinates using Kobamin [21] and validated using PROCHECK [22]. The 3D structure of neolignan compounds as ligands was built with the ChemDraw Ultra 7.0 program [23] to prepare the 3D structure used in QSAR and molecular docking analyses. The ligand conformational energies were minimized using the MMFF94 force field. All 3D structures of hESR-1 proteins and the ligands were stored in PDB format, 3D structure formats with the standard atomic coordinates of biomolecules.

Molecular Docking of lignan complex compounds and their derivatives with hESR-1

Molecular docking analysis was carried out by the Autodock Vina program (Vina, The Scripps Institute) [24, 25]. AutodockTools are used for protein preparation, such as setting the electron charge amount and compiling polar hydrogen compounds [26]. Ligands prepared have adjustable angles. The proteins and ligands are then stored in pdbqt format, a format with specific extensions that store atomic coordinates, partial charges, and atomic types identified explicitly by the molecular docking Autodock Vina program. Determination of specific molecular docking between hESR-1 and lignan produces bond energy involving total intermolecular energy (kcal/mol), including hydrogen bond energy, Van der Waals energy, dissolved energy, and electrostatic energy. Analysis of interactions between ligands and target proteins was carried out using Ligplot+ [27].

Analysis of lignan compounds and their derivatives based on Quantitative Property Relationship (QSPR)

The 3D lignan structure and its derivatives were analyzed based on physicochemical properties using the Molsoft Drug-Likeness program [28]. Determining these physicochemical properties is essential in developing drug candidates at every stage, from design studies to pre-clinical trials. Drug properties such as absorption, distribution, metabolism, and excretion (ADME) must be considered in drug development. Identification of ADME in the early stages will bring the compound to drug screening. Unwanted properties of the compound will cause failure in drug development. Prediction of ADME properties of drug candidate compounds had used ACD/I-lab [29] and FAF-Drugs3 programs [30]. In this study, neolignan compounds were analyzed for ADME properties based on oral bioavailability, volume distribution, absorption into the digestive tract, and evaluation of plasma binding proteins.

Cell culture and antiproliferative assay

The breast cancer, MCF-7 cell lines were used in this study (American Type Cell Collection, ATCC). The cells were cultured using RPMI 1640 culturing media (PAA, Leverkusen, Germany). Trypsin was added to cells to hydrolyze the protease after cells reached 80% confluent, and cells were then counted using a hemocytometer and plated in a microtiter plate of 96-wells. Incubation was done for overnight to allow cell attachment following to change the medium. The amount of 0.2 mL of new supplemented medium was added into each well. The cells were then treated with lignan and its derivative at different concentrations and incubated at 37°C, 5% CO_2 for 24 h. Each concentration of the samples was measured in triplicate. The colorimetric assay was performed at an absorbance of 570 nm. The results were expressed as a percentage of control, giving a certain percentage of cell viability after 24 h exposure to the isolated lignans. The inhibition of cell growth by isolated lignans was expressed as a percentage of antiproliferative value [31].

RESULTS AND DISCUSSION

Isolation and identification of neolignan from P. declinata leaves

We had successfully done isolating the plant neolignans: aristolgol (**R1**) and aristoligone (**R2**) with purity > 95% from approximately 3 kg dried leaf powder sample of *P. declinata* Nees by maceration in 15 L n-hexane for 24 hours and repeated three times. The extract samples were evaporated and yielded 83.4 g of n-hexane extract. The residue was macerated with 15 L dichloromethane (DCM), followed by evaporation and the final yield was 163.8 g of DCM extract. The remaining residue from DCM extraction was macerated with 15 L methanol then evaporated to produce 367.8 g of methanolic extract. DCM extract was purified by flask silica column chromatography using an eluent mixture of n-hexane and DCM gradient to purify compound R1 (25 mg) and R2 (53 mg). Each of them was identified and tested for its activity against cancer cell lines (MCF-7). The purified compounds R1 and R2 were identified as neolignan derivatives, respectively, using ^{1}H-^{13}C NMR Spectroscopy to determine the relationship between structure and activity. The identified structure of **R1** and **R2** are depicted in Figure 1.

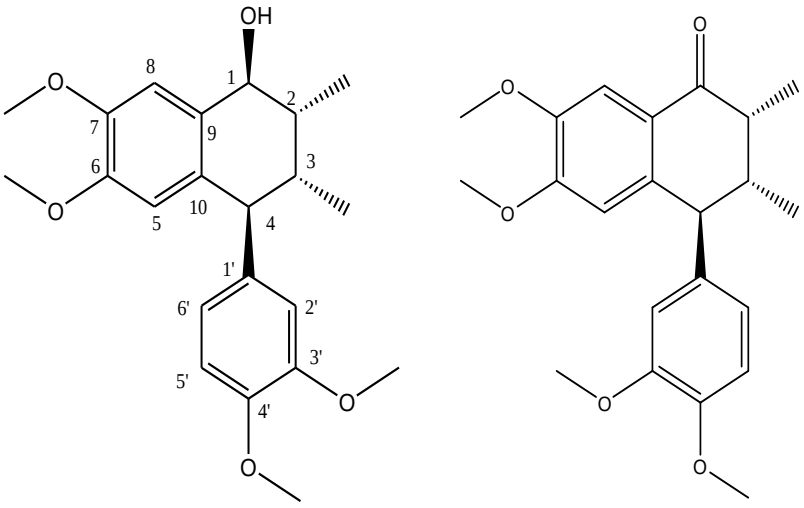

Figure 1. Molecular structure of: a. aristoligol (**R1**) and b. aristoligone (**R2**).

These two neolignans are naturally produced from *P. declinata* leaves as secondary metabolites. The lignan structures were identified by using ^{1}H-^{13}C NMR Spectroscopy and LC-MS. The chemical structure elucidation of compound **R1** with spectral NMR HMBC is shown in Figure 2. Meanwhile, structure elucidation of compound **R2** and reduced-aristoligol are depicted in Figure 3.

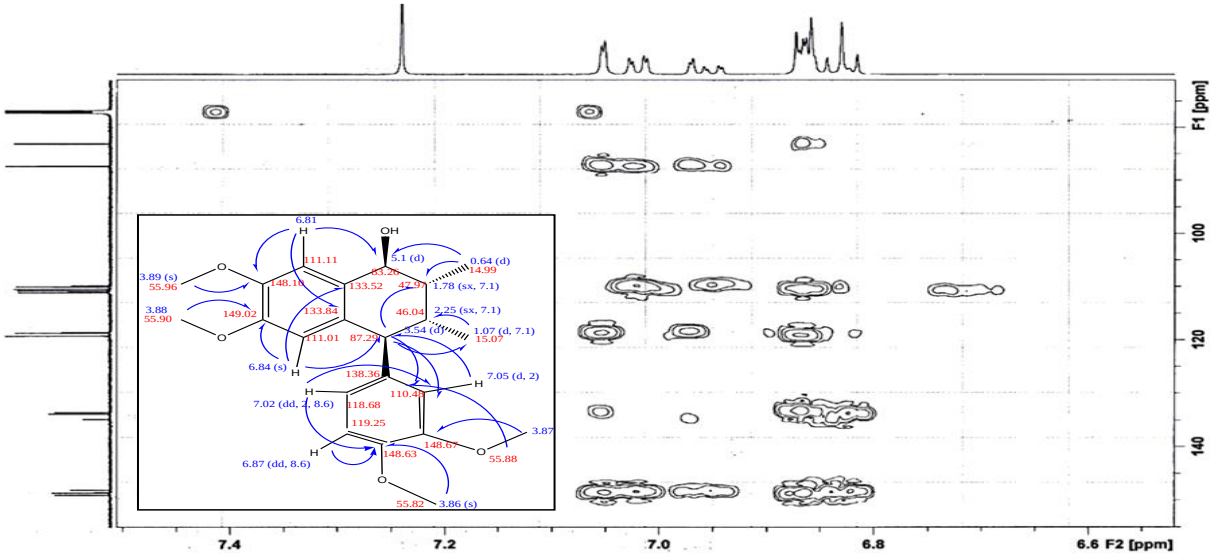

Figure 2. Identified structure of aristoligol compound **R1** with spectral NMR HMBC. Red highlights are proton NMR chemical shifts, and blue highlights are carbon NMR chemical shifts.

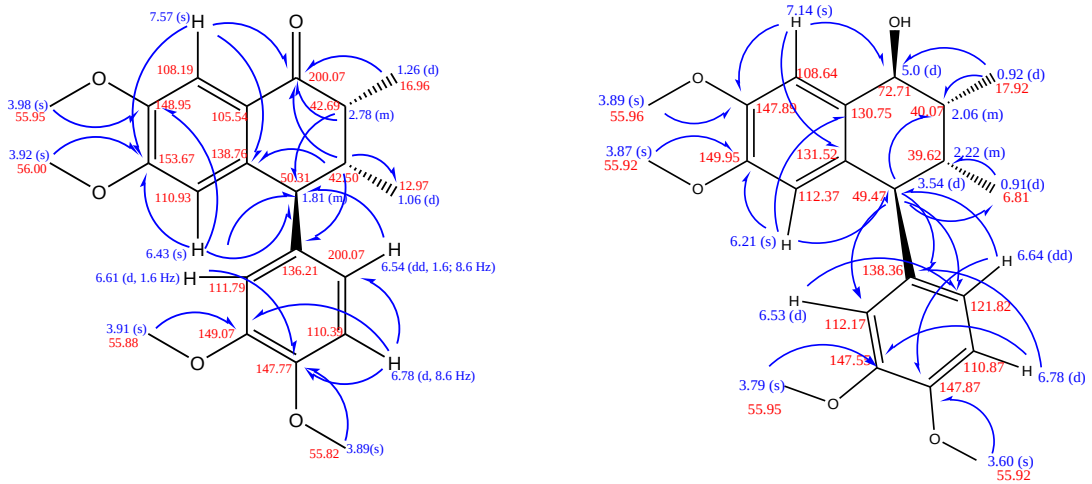

Figure 3. Identified structure of a. aristoligone compound **R2**; b. reduced-aristoligol with spectral NMR HMBC. Red highlights are proton NMR chemical shifts, and blue highlights are carbon NMR chemical shifts.

The chemical shifts for ^{1}H (500 MHz) and ^{13}C-NMR (125 MHz) spectrum between compound **R1** and **R2** are listed in Table 1, while the chemical shifts for ^{1}H (500 MHz) and ^{13}C-NMR (125 MHz) spectrum between compound **R2** and reduced-aristoligol are listed in Table 2.

Table 1. Comparison of chemical shift data for ^{1}H (500 MHz) and ^{13}C-NMR (125 MHz) spectrum for **R1** and **R2** compounds in $CDCl_3$ (δ in ppm, J in Hz).

No	**Aristoligol (R1)**		**Aristoligone (R2)**	
	δ_H (in ppm, J in Hz)	**δ_C***	**δ_H (in ppm, J in Hz)**	**δ_C***
1	5.1 (d, 8.6)	83.26	-	200.07
2	1.78 (sextet, 7.1)	47.97	2.78 (m, 7.1)	42.69
2-CH_3	0.64 (d, 7.0)	14.99	1.26 (d, 7.1)	15.07
3	2.25 (sextet, 7.1)	46.04	2.43 (m, 7.1)	42.50

3-CH_3	1.07 (d, 7)	15.07	1.07 (d, 7)	16.96
4	4.41 (d, 9)	87.29	1.81 (m)	50.31
5	6.84 (s)	111.01	6.43 (s)	110.93
6	-	149.02	-	153.67
6-OCH_3	3.88 (s)	55.90	3.92 (s)	56.0
7	-	148.10	-	148.95
7-OCH_3	3.89 (s)	55.96	3.98 (s)	55.95
8	6.81 (s)	111.11	7.57 (s)	108.10
9	-	133.52	-	125.54
10	-	133.84		138.76
1’	-	134.87	-	136.21
2’	7.05 (d, 2)	110.48	6.54 (dd, 1.6; 8.6)	121.09
3’	-	148.67	6.78 (d, 8.6)	110.39
4’-OCH_3	3.87 (s)	55.88	3.89 (s)	55.82
5’		148.63	-	149.07
5’-OCH_3	3.86 (s)	55.82	3.91 (s)	55.88
6’	6.87 (d, 8)	119.25	6.61 (d, 1.6)	111.79

* Proton – carbon correlation based on HMQC experiment.

Compound **R1** and **R2** were isolated as amorphous solids. The mass spectrums showed the molecular ion peaks of **R1** at m/z = 373,2003 $[M+H]^+$ and **R2** at m/z = 371,1849 $[M+H]^+$. Thus suggesting that **R1** and **R2** have molecular formulas of $C_{22}H_{29}O_5$ and $C_{22}H_{28}O_5$, respectively. The ^{1}H-NMR for these neolignans showed a pair of doublet peaks at δ 0.64 and 1.07 ppm, continued by δ 1.26 ppm and 1.07 ppm that correspond to the methyl groups at positions C-2 and C-3 of compound **R1** and **R2**, respectively. The sharp singlet peaks at δ 6.84 ppm and δ 6.87 ppm (**R1**) followed by δ 6.43 ppm and δ 6.61 ppm (**R2**) belong to the H-5 and H-6’, respectively on the benzene rings. The aliphatic protons of ring B for both compound **R1** and **R2** resonated as sextets at **R1** with δ 1.78 to 2.25 ppm and multiplets at R2 with δ 1.81 to 2.78 ppm, respectively. To reinforce this expectation, the comparison of chemical shift data for ^{1}H (500 MHz) and ^{13}C-NMR (125 MHz) spectrum for **R1** and **R2** carried out as shown in Table 1. Based on the literature, long-distance correlation (HMBC) measurements have demonstrated the compound similarity as 4-epi-aristoligone isolated from *Aristolochia chilensis* and *Holostylis reniformis* plants [32-34].

The ^{13}C-NMR spectrum of **R1** and **R2** showed the presence of twenty-two carbons, which are in agreement with the molecular formula $C_{22}H_{29}O_5$ and $C_{22}H_{28}O_5$, respectively. The DEPT spectrum showed the presence of two-methyl and four-oxy-methyl, nine methines, and seven quaternary carbons. The methyl groups of **R1** resonated at δ 14.99 ppm and δ 15.07 ppm for C-2 and C-3, respectively. Meanwhile, the methyl groups of **R2** resonated at δ 42.69 ppm and δ 16.96 ppm for C-2 and C-3, respectively. Moreover, the oxy-methyl groups of **R1** and **R2** resonated between δ 55.90 to δ 56.0 ppm. The characteristic quaternary carbon peak C-1 appeared at δ 83.26 ppm for **R1** and δ 200.07 ppm for **R2,** indicating specifically attach to hydroxyl (R1) ketone (**R2**) groups, respectively. The complete backbone and side-chain assignments of all protons and carbons of **R1** and **R2** were shown in Table 3.

Synthesis of aristoligone derivatives

Compound **R2** was synthesized using $NaBH_4$ in methanol to produce a transition compound, the reduced-aristoligol. The reduced-aristoligol was then further synthesized to produce the acetyl aristoligol compound (**R3**). The synthetic route of the target compounds **R2** to **R3** is shown in Scheme 1. hydrogenation of **R2** compound and esterification (acetylation) of the reduced-aristoligol compound using acetic anhydride and DMAP as a catalyst in chloroform ($CHCl_3$) were also carried out. The ^{1}H and ^{13}C-NMR spectrum of compound **R2** indicated the presence of three aromatic protons with ABC system appear at δ_H 1.26 (d, 7.1 Hz); 1.07 (d, 7 Hz) and 6.61 (d, 1.6 Hz), as illustrated in ring C. Two aromatic protons in singlet form were shown at δ_H 6.43 (s) and 7.57 (s), and four methoxyl groups (s) at δ_H 3.92; 3.98; 3.89 and 3.91 at C-6, C-7, C-4’ and C-5’, respectively. The presence of two methyl groups (d) and three methine CH (m) were shown at δ_H 1.26, 1.07, and 2.78. It was characterized as a lignan derivative of aristoligone (**R2**). Supporting data such as ^{13}C-NMR and H-C correlation (HMQC) spectrum, with the presence of carbonyl group at δ_H 200.07, were illustrated in Figure 3. For a complete structure, it was confirmed that the HMBC experiment detected the position of chemical

shifts. Based on these results and compared to some references, this compound has a structure lignan derivative, as aristoligone (**R2**) [35].

Looking at further identification of compound **R2** was reduced in excess of $NaBH_4$/methanol**.** It was crystallized in n-hexane and DCM mixture solution to result in a colorless crystal reduced-aristoligol compound in a good yield as a pure crystal of reduced-aristoligol (100%). Reduced-aristoligol was considered as an intermediate compound before producing the end product. Mass spectroscopy data supported compound reduced-aristoligol elucidation, with the presence of molecular ion at m/z $(M+H)^+$ = 373.12. The ^{1}H-NMR spectrum indicated a new methine hydroxy (HC-OH) at δH 5.0 (d, 7.5) and the carbonyl group disappearance in the ^{13}C-NMR spectrum. The measurement of 2D-NMR (HMQC and HMBC experiments) was used to support a complete assignment. The comparison of chemical shift data between compound **R2** and reduced-aristoligol was assigned under the same parameter as shown in Table 2. Meanwhile, the molecular structure of reduced-aristoligol elucidation is depicted in Figure 4.

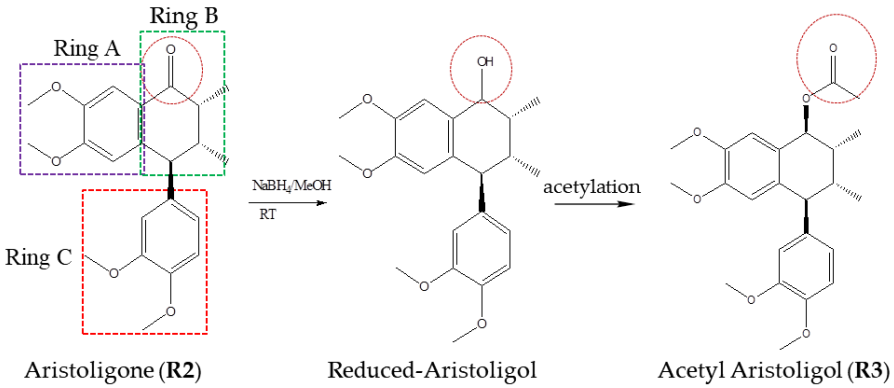

Scheme 1. The synthetic route of aristoligone derivatives. Reduced-aristoligol as the intermediate compound was synthesized in reduction process from **R2** resulting hydroxyl group from ketone substitution. Moreover, the reduced-aristoligol compound was acetylated and yielded acetyl aristoligol compound, **R3**.

Table 2. Comparison of chemical shift data for ^{1}H (500 MHz) and ^{13}C-NMR (125 MHz) spectrum for **R2** in CD_3OD and reduced-aristoligol compounds in $CDCl_3$ (δ in ppm, J in Hz).

No	Aristoligone (R2)		Reduced-Aristoligol	
	δ_H (in ppm, J in Hz)	**δ_C***	**δ_H (in ppm, J in Hz)**	**δ_C***
1	6.15 (d, 4.6)	76.94 (d)	5.0 (d, 7.5)	72.71 (d)
2	2.07 (m)	39.76 (d)	2.06 (m, 7.5)	40.07 (d)
2-CH_3	0.87 (d, 6.5)	17.34 (q)	0.92 (d, 7.1)	17.92 (q)
3	2.35 (m)	35.38	2.22 (sx, 7.1)	39.62 (d)
3-CH_3	0.94 (d, 6.5)	8.70	0.91 (d, 7.1)	6.81 (q)
4	3.62 (d, 6.5)	49.64	3.54 (d, 7.1)	49.47 (d)
5	6.72 (s)	109.03	7.14 (s)	108.64 (d)
6	-	148.46	-	148.95 (s)
6-OCH_3	3.84 (s)	55.90	3.87 (s)	55.92 (q)
7		147.52	-	147.89 (s)
7-OCH_3	3.86 (s)	55.98	3.89 (s)	55.96 (q)
8	6.26 (s)	111.95	6.21 (s)	112.37 (d)
9	-	131.71	-	130.73 (s)
10	-	126.66	-	131.52 (s)

1’	-	138.19	-	138.36 (s)
2’	6.51 (d, 2.5)	110.80	6.53 (d, 2)	112.17 (d)
3’	-	148.46	-	147.55 (s)
3’-OCH_3	3.85 (s)	55.84	3.79 (s)	55.95 (q)
4’	-	148.93	-	147.56 (s)
4’-OCH_3	3.61 (s)	49.64	3.60 (s)	55.92 (q)
5’	6.78 (d, 7.6)	109.03	6.78 (d, 8)	110.87 (d)
6’	6.57 (bd, 7.6)	121.63	6.64 (dd, 2; 8)	121.83 (d)

*Proton – carbon correlations based on HMQC experiment.

Furthermore, the evaluation of correlation functional group (hydroxyl group) and biological activity, reduced-aristoligol was acetylated with the excess of acetic anhydride and catalyst N, N-dimethylaminopyridine (DMP) in chloroform. After purification, the **R3** compound was obtained in colorless crystal in 98% yield. The molecular weight of **R**3 was determined by mass spectroscopy, and it was identified to have MW = 414.20. The spectrum of ^{1}H-NMR and ^{13}C-NMR appeared a specific signal for the acetyl group at δ 2.19 (s); 21.49 and 171.36. The other chemical shift of methine hydroxy (H-C-OR) moved to the downfield area at δ 6.15 (H-1, d, J = 4.53 Hz) and 76.94, indicating that compound **R3** was known as acetyl aristoligol, as shown in Table 3. The elucidated molecular structure of compound **R3** with spectral NMR HMBC is depicted in Figure 4. Furthermore, compounds **R1, R2,** and **R3** were determined by their QSAR properties and molecular modeling.

Table 3. Comparison of chemical shift data for ^{1}H (500 MHz) and ^{13}C-NMR (125 MHz) spectrum for reduced-aristoligol in CD_3OD and **R3** compounds in $CDCl_3$ (δ in ppm, J in Hz).

No	**Reduced-Aristoligol**		**Acetyl Aristoligol (R3)**	
	δ_H (in ppm, J in Hz)	**δ_C***	**δ_H (in ppm, J in Hz)**	**δ_C***
1	5.0 (d, 7,5)	72.71 (d)	6.15 (d, 4.6)	76.94 (d)
2	2.06 (m, 7.5)	40.07 (d)	2.07 (m)	39.76 (d)
2-CH_3	0.92 (d, 7.1)	17.92 (q)	0.87 (d, 6.5)	17.34 (q)
3	2.22 (sx, 7.1)	39.62 (d)	2.35 (m)	35.38
3-CH_3	0.91 (d, 7.1)	6.81 (q)	0,94 (d, 6.5)	8.70
4	3.54 (d, 7,1)	49,47 (d)	3.62 (d, 6.5)	49.64
5	7.14 (s)	108.64 (d)	6.72 (s)	109.03
6	-	148.95 (s)	-	148.46
6-OCH_3	3.87 (s)	55.92 (q)	3.84 (s)	55.90
7	-	147.89 (s)		147,52
7-OCH_3	3.89 (s)	55.96 (q)	3.86 (s)	55,98
8	6.21 (s)	112.37 (d)	6.26 (s)	111.95
9	-	130.73 (s)	-	131.71
10	-	131.52 (s)	-	126.66
1’	-	138.36 (s)	-	138.19

2’	6.53 (d, 2)	112.17 (d)	6.51 (d, 2.5)	110.80
3’	-	147.55 (s)	-	148.46
3’-OCH_3	3.79 (s)	55.95 (q)	3.85 (s)	55.84
4’	-	147.56 (s)	-	148.93
4’-OCH_3	3.60 (s)	55.92 (q)	3.61 (s)	49.64
5’	6.78 (d, 8)	110.87 (d)	6.78 (d, 7,6)	109.03
6’	6.64 (dd, 2; 8)	121.83 (d)	6.57 (bd, 7.6)	121.63
C=O	-	-	-	171.36
CH_3CO-	-	-	2.19 (s)	21.49

*Proton – carbon correlations based on HMQC experiment.

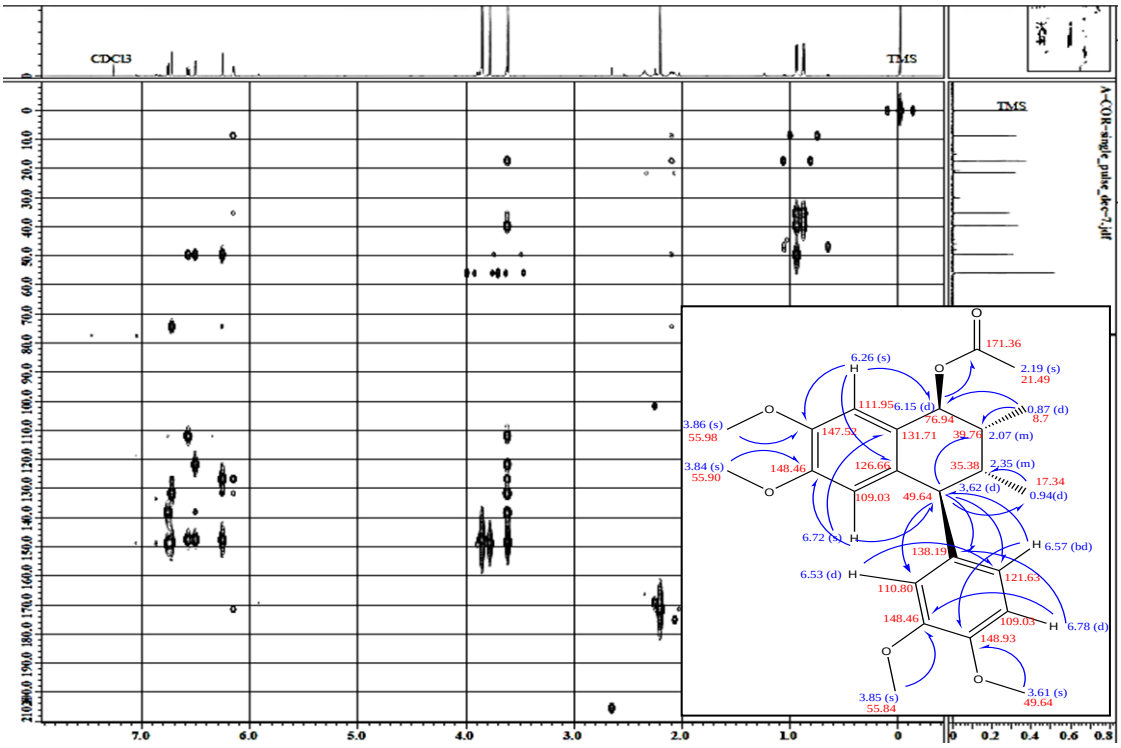

Figure 4. Identified structure of acetyl aristoligol compound (**R3**) with spectral NMR HMBC.

Analysis of Lignan compounds and their derivatives based on Quantitative Structure-Activity Relationship, (QSPR)

The structure of the three-dimensional lignan compounds (**R1** and **R2**) are natural material compounds isolated from the *P. declinata* Nees plant, and its derivative (**R3**) have been synthesized, where the difference in structure between lignans and its derivatives were based on the isomer of aristoligone (**R2**) hydroxyl side chain into ketone from aristoligol isolate compound. The reduced-aristoligol is an isomer of aristoligol (**R1**). Acetyl aristoligol (**R3**) has an ester side group as a product from acetylation of the reduced-aristoligol. The analysis of lignan compounds and their derivatives was carried out based on physicochemical and drug-likeness properties (Table 4 and Table 5).

Table 4. Physico-chemical properties of ligan and its derivatives.

Compound	HB* Donor	HB* Acceptor	Molecular weight	Bond rotation	Refractory index	Density (g/cm^3)	Surface tension (dyne/cm)
R1	1	3	372.20	5	1.567	1.148	47.30
R2	1	3	370.18	5	1.57	1.102	43.90
R3	0	6	414.20	5	1.531	1.016	39.60

*HB = *Hydrogen bond*

Table 5. Drug likeness properties of the ligand and its derivatives as anticancer.

Compound	Drug Likeness Score**	Log P**	Solubility (mg/L)*	TPSA***	Stereocenter amount**	Lipinski Rule Violation**
R1	0.53	1.93	210.05	43.86	0	0
R2	0.53	1.93	210.05	43.86	0	0
R3	0.58	5.08	6.33	50.56	4	1

**Molsoft Drug-likeness
***FAF-Drugs3

Based on the physicochemical analysis of lignans and their derivatives, there were variations in the three compound intrinsic properties. **R1** and **R2** have one hydrogen bond donor, while **R3** does not have it. Moreover, R1 and R2 have three hydrogen bond acceptors, while R3 has six hydrogen bond acceptors. All lignan has five bond rotations. The range of the refractory index is between 1.533 - 1.567, the density range of the four compounds is at 1.102 - 1.240 g/cm^3, and the surface tension is in the range of 43.5 - 47.3 dyne/cm., Furthermore, the results of the drug-likeness analysis showed that the compound **R1, R2,** and **R3** meet all the criteria of Lipinski's rules of five (Ro5) where **R1** and **R2** have no drug-likeness violation were found, except **R3** that has a log P value slightly higher than 5, where log P value should be ≤ 5 [36].

Table 6. ADME properties of lignans as hESR-1 inhibitors.

Compound	Oral Bioavailability	Distribution volume (L/kg)	% Maximum absorption of the jejunum	Absorption type	% Plasma binding protein
R1	Good	1.62	100	Transcelullar	83.45
R2	Good	2.04	100	Transcelullar	82.76
R3	Good	2.32	100	Transcelullar	83.97

Further analysis of determining the adsorption-metabolism-excretion (ADME) properties of drug candidates in the human body is critical to evaluating body organs and tissue [37, 38]. In this study, the results of the determination of ADME assessment in silico [39-41] showed that good oral bioavailability and distribution volume in the range of 1.62 - 2.32 L/kg of the three compounds (Table 6). The percentage of maximum jejunal absorption of the four compounds was also found to reach 100% with the type of absorption via the transcellular pathway. The percentage of plasma binding proteins in the three compounds are in the range of 82.76 - 83.97%, where **R2** has the lowest fraction of protein in blood plasma compared to other lignan compounds. It indicates that most of the **R2** fraction compound not bound in blood plasma protein will be carried into the body metabolic system until the excretion stage, then the drug level accumulates in the body becomes smaller compared to the other two compounds. Thus, **R2** is considered to have the best ADME properties due to it has the lowest risk of toxicity in the body. The successful drug assessment in silico was also performed at up to 50,000 compounds from public or corporate databases, which were applied to predict and visualize fragmental contributions to guide further drug discovery and design [42].

Molecular Docking of lignan-hESR-1 complexes

In determining the interaction of lignan compounds and their derivative, molecular docking analysis is used to determine the specific interactions between ligands, lignan compounds, and their derivative with the target protein hESR-1. Based on the results of the docking, it was found that compounds: **R1** (yellow), **R2** (cyan), and **R3** (magenta) had different binding sites at the hESR-1 binding pocket (Figure 6).

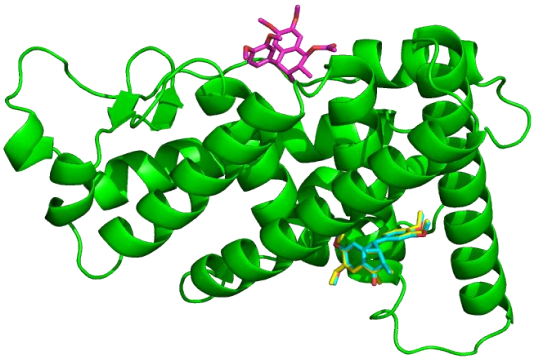

Figure 5. Molecular docking of hESR-1 with ligands: **R1** (yellow), **R2** (cyan), and **R3** (magenta).

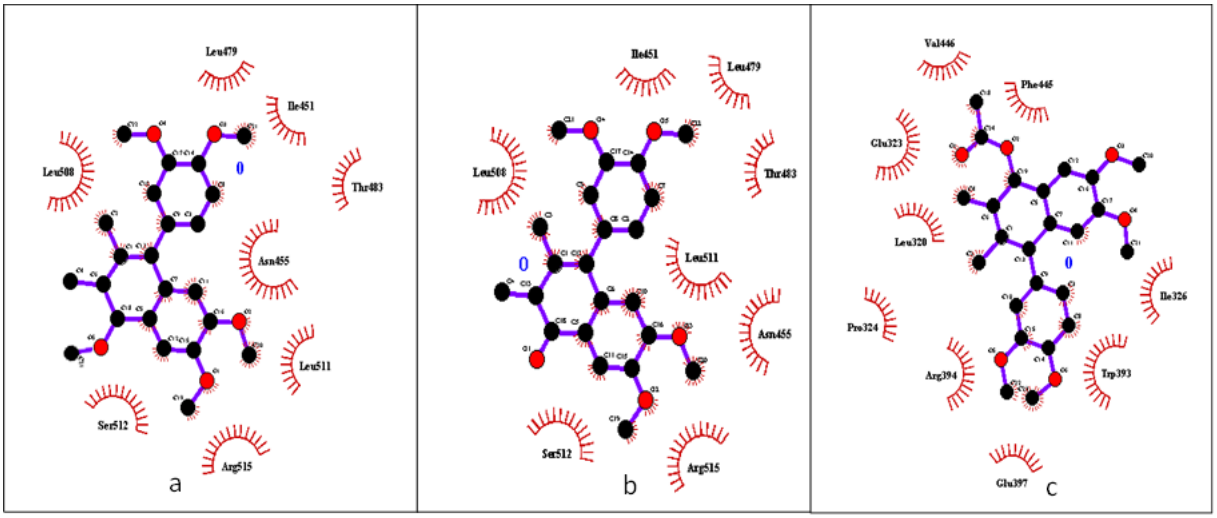

Figure 6. Chemical interactions of: (a) ESR residue–**R1** interaction; (b) ESR residue–**R2** interaction; c) ESR residue –**R3** interaction.

Table 7. Summary of molecular docking analysis.

Compound	Binding affinity (kcal/mol)	Amino acid residue involved in protein-ligand interaction	∑ hydrogen bond	Ki value (nM)
R1	-6.6	Leu479, Ile451, Asn455, Leu511, Arg515, Ser512, Leu508, Thr483	0	1.43×10^{-5}
R2	-6.7	Leu479, Ile451, Asn455, Leu511, Arg515, Ser512, Leu508, Thr483	0	1.21×10^{-5}
R3	-6.2	Val446, Glu323, Leu320, Pro324, Arg394, Glu397, Trp393, Ile326, Phe455	0	2.82×10^{-5}

The interaction of **R1**, **R2,** and **R3** compounds with specific amino acid residues at hESR-1 was stabilized by hydrophobic interactions (Figure 6). Based on the docking interaction results, where the binding energy value and inhibition constants are obtained that **R2** compounds have the highest inhibitory ability compared to compounds **R1** and **R3** (Table 7). The in silico study result showed that the **R2** compound could be used as a potential candidate for the anticancer agent. This research requires further testing in vitro and in vivo as a step to validate the activity of **R2** compound in living cells. The antiproliferative activities of compound **R1**, **R2,** and **R3** against MCF-7 cell lines are depicted in Figure 7. It showed that **R1** has the highest antiproliferative activity at 25 µg/mL or 30×10^{-3} µM, followed by **R2** and **R3**, respectively. The IC_{50} values from compounds **R1**, **R2,** and **R3** are depicted in Figure 8. The microscopic observation of MCF-7 cell lines lysis after treatments of **R1**, **R2,** and **R3** are shown in Figure 9. These neolignan compounds showed potent cell lysis capacities.

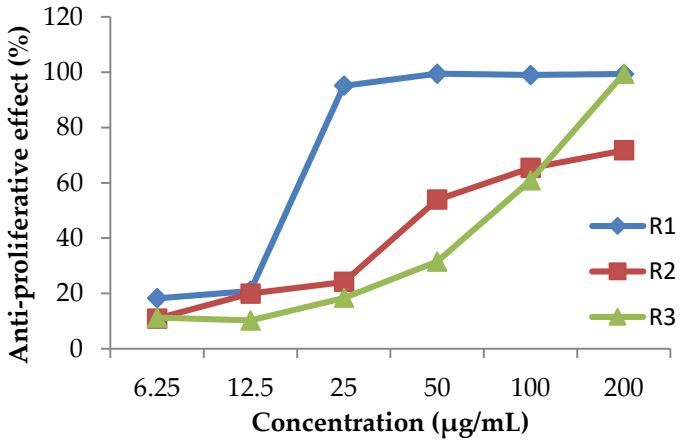

Figure 7. The graph-trend of the antiproliferative effect of compound **R1**, **R2,** and **R3** against MCF-7 cell lines.

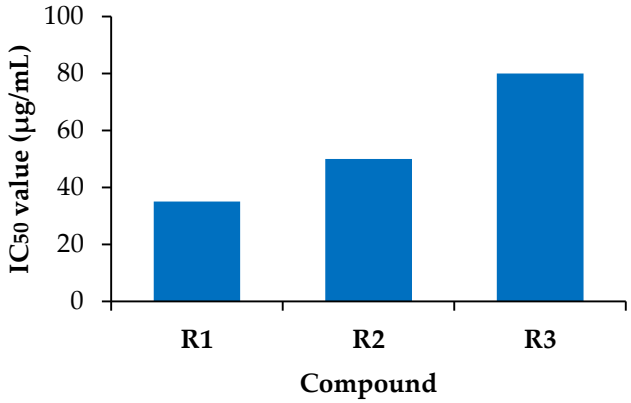

Figure cell lines.

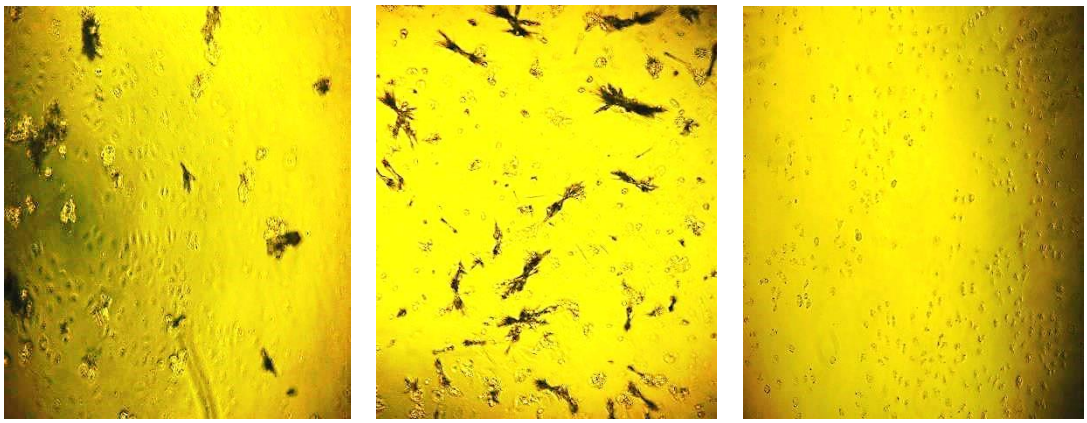

Figure 9. Microscopic appearance of cell lysis (MCF-7 cell lines) due to treatment of a. compound **R1**; b. compound **R2**; c. compound **R3**.

There are several factors for a failed drug, mainly due to adsorption, distribution, metabolism, and excretion (ADME). It can be overcome by following Lipinski's rule of five (Ro5). According to Lipinski's rule that the activity of a compound is influenced by several factors, including the number of hydrogen bond donors should not be more than 5, lipophilicity with a Log P value < 5, molecular weight (MW) < 500, and the number of hydrogen bond acceptors <10, where the MW of **R1** is 372,2 with Log P 3.99 and MW of **R2** is 370.18 with Log P 3.9 [36, 43]. Besides that, it was found that **R3** (MW = 414.20) has a log P value slightly higher than 5, while two other neolignans were way lower than 5, which assumed that the log P value over than five could cause the decrease of solubility [44]. Moreover, the change in carbonyl group into hydroxy and ester groups from a calanone can increase its activity against colon cancer, HCT116 from IC_{50} > 20 µg/ml to 1.28 µg/ml; whereas for P388 cancer cells from IC_{50} value of 13.50 to 7.25 µg/ml (31.81 $x10^{-3}$ to 17.08$x10^{-3}$ µM) [45]. The cytotoxic activity of **R1** has the lowest value of IC_{50} (94$x10^{-3}$ µM) among three neolignans (Figure 8), which indicated that **R1** has the best inhibition activity to MCF-7 breast cancer cell lines. The microscopic appearance of cell lysis (MCF-7 cell lines) due to treatments of **R1**, **R2,** and **R3** are shown in Figure 9. Our study demonstrated that these neolignan compounds have potent cell lysis capacities. It is

believed that the hydroxyl and carbonyl groups of lignans have critical roles in inhibiting cancer cell proliferation [46-48]. Thus, these neolignans will have high implications in biomedical applications, especially in treating cancers.

CONCLUSION

Neolignan compounds from *P. declinata* Nees leaves have been successfully isolated as aristoligol (**R1**) and aristoligone (**R2**). The synthesis of aristoligone (**R2**) by reducing agent resulted in reduced-aristoligol as an intermediate compound, following synthesis by acetylation (esterification) resulted from end product of acetyl aristoligol (**R3**) as new lignan. Aristoligone (**R2**) reduction by $NaBH_4$/MeOH reduction resulted from pure reduced-aristoligol in high yield (100%), following acetylation with Ac_2O/DMAP in $CHCl_3$ also provided a high yield of acetyl aristoligol, **R3** (98%). R1 performed the best antiproliferative and cytotoxic activities. A hydroxyl group is an essential group in inhibiting the growth of cancer cells (chromophore groups), which plays a significant role in hydrogen bonding in inhibiting ESR1 enzyme in silico, reinforced by a small interaction energy value capable of stabilizing the interaction between binding pocket residues of hESR-1 with neolignan derivatives of **R1, R2** and **R3**.

ACKNOWLEDGEMENT

The authors would like to thank BOPTN Kemenristekdikti and DRPM Universitas Indonesia for the financial support of our research. We also would like to thank the Research Center for Chemistry, the Indonesian Institute of Sciences; and the University of Malaya, Malaysia, for providing research facilities and instruments.

REFERENCES

1. J. Zhu, L. Yan, X. Xu, Y. Zhang, J. Shi, C. Jiang, D. Shao. (2018). Strategies to enhance the production of pinoresinol and its glucosides by endophytic fungus (Phomopsis sp. XP-8) isolated from Tu-chung bark, *AMB Express* 8(1), 55.
2. W. Ding, N. Liping, H. Xing, Z. Wei, Q. Zhoua, R. Nong, J. Chen. (2018). Essential oil extracted from leaf of Phoebe bournei (Hemsl.) yang: chemical constituents, antitumor, antibacterial, hypoglycemic activities, *Natural Product Research*, 1-4.
3. D.S. Kumar, R.S. Badoni. (2013). Ethnobotany, pharmacology and phytochemistry of the genus Phoebe (Lauraceae), *J Mini-Reviews in Organic Chemistry* 10(1), 12-26.
4. H. Omar, N.M. Hashim, A. Zajmi, N. Nordin, S.I. Abdelwahab, A.H. Azizan, A.H. Hadi, H.M. Ali. (2013). Aporphine alkaloids from the leaves of Phoebe grandis (Nees) Mer. (Lauraceae) and their cytotoxic and antibacterial activities, *Molecules* 18(8), 8994-9009.
5. C. Charalambous, C.A. Pitta, A.I. Constantinou. (2013). Equol enhances tamoxifen's antitumor activity by induction of caspase-mediated apoptosis in MCF-7 breast cancer cells, *BMC cancer* 13(1), 238.
6. S.M. Mense, T.K. Hei, R.K. Ganju, H.K. Bhat. (2008). Phytoestrogens and breast cancer prevention: possible mechanisms of action, *Environ Health Perspect* 116(4), 426-33.
7. I. Bilal, A. Chowdhury, J. Davidson, S. Whitehead. (2014). Phytoestrogens and prevention of breast cancer: The contentious debate, *World J Clin Oncol* 5(4), 705-12.
8. H. Jiang, J. Fan, L. Cheng, P. Hu, R. Liu. (2018). The anticancer activity of genistein is increased in estrogen receptor beta 1-positive breast cancer cells, *Onco Targets Ther.* 11, 8153.
9. A. Hadjisavvas, M.A. Loizidou, N. Middleton, T. Michael, R. Papachristoforou, E. Kakouri, M. Daniel, P. Papadopoulos, S. Malas, Y. Marcou, K. Kyriacou. (2010). An investigation of breast cancer risk factors in Cyprus: a case control study, *BMC Cancer* 10, 447.
10. H. Xin, Y. Kong, Y. Wang, Y. Zhou, Y. Zhu, D. Li, W. Tan. (2013). Lignans extracted from Vitex negundo possess cytotoxic activity by G2/M phase cell cycle arrest and apoptosis induction, *Phytomedicine* 20(7), 640-7.
11. G. Momekov, D. Yossifov, M. Guenova, A. Michova, N. Stoyanov, S. Konstantinov, T. Ionkov, P. Sacheva, I. Ionkova. (2014). Apoptotic mechanisms of the biotechnologically produced arylnaphtalene lignan justicidin B in the acute myeloid leukemia-derived cell line HL-60, *Pharmacol. Rep.* 66(6), 1073-6.
12. J. Kuusipalo, Y. Jafarsidik, G. Ådjers, K.J.F.E. Tuomela, Management. (1996). Population dynamics of tree seedlings in a mixed dipterocarp rainforest before and after logging and crown liberation, 81(1-3), 85-94.
13. B. Elya, B. Katrin, R.C. Forestrania, R. Sofyan, R.A. Chandra. (2017). Alkaloid from Phoebe declinata Nees Leaves, *Pharmacognosy Journal* 9(6), 713-720.
14. A.J.G.H. Kostermans. (1957). Lauraceae, *Reinwardtia* 4(2), 193-256.
15. L.S. Velentzis, J.V. Woodside, M.M. Cantwell, A.J. Leathem, M.R. Keshtgar. (2008). Do phytoestrogens reduce the risk of breast cancer and breast cancer recurrence? What clinicians need to know, *Eur J Cancer* 44(13), 1799-806.
16. L. Molina, F.A. Bustamante, K.D. Bhoola, C.D. Figueroa, P. Ehrenfeld. (2018). Possible role of phytoestrogens in breast cancer via GPER-1/GPR30 signaling, *Clin Sci* 132(24), 2583-2598.
17. Y. Peng, Z.-B. Luo, J.-J. Zhang, L. Luo, Y.-W. Wang. (2013). Collective synthesis of several 2, 7′-cyclolignans and their correlation by chemical transformations, *Organic & Biomolecular Chemistry* 11(43), 7574-7586.
18. Y. Li, S. Xie, J. Ying, W. Wei, K. Gao. (2018). Chemical structures of lignans and neolignans isolated from Lauraceae, *Molecules* 23(12), 3164.
19. T.D. Goddard, C.C. Huang, T.E. Ferrin. (2005). Software extensions to UCSF chimera for interactive visualization of large molecular assemblies, *Structure* 13(3), 473-82.
20. E.F. Pettersen, T.D. Goddard, C.C. Huang, G.S. Couch, D.M. Greenblatt, E.C. Meng, T.E. Ferrin. (2004). UCSF Chimera--a visualization system for exploratory research and analysis, *J. Comput. Chem.* 25(13), 1605-12.
21. J.P. Rodrigues, M. Levitt, G. Chopra. (2012). KoBaMIN: a knowledge-based minimization web server for

protein structure refinement, *Nucleic Acids Res* 40(Web Server issue), W323-8.
22. R.A. Laskowski, J.A. Rullmannn, M.W. MacArthur, R. Kaptein, J.M. Thornton. (1996). AQUA and PROCHECK-NMR: programs for checking the quality of protein structures solved by NMR, *J. Biomol. NMR* 8(4), 477-86.
23. Z. Li, H. Wan, Y. Shi, P. Ouyang. (2004). Personal experience with four kinds of chemical structure drawing software: review on ChemDraw, ChemWindow, ISIS/Draw, and ChemSketch, *J Chem Inf Comput Sci* 44(5), 1886-90.
24. D. Seeliger, B.L. de Groot. (2010). Ligand docking and binding site analysis with PyMOL and Autodock/Vina, *J. Comput. Aided Mol. Des.* 24(5), 417-22.
25. O. Trott, A.J. Olson. (2010). AutoDock Vina: improving the speed and accuracy of docking with a new scoring function, efficient optimization, and multithreading, *J. Comput. Chem.* 31(2), 455-61.
26. N. El-Hachem, B. Haibe-Kains, A. Khalil, F.H. Kobeissy, G. Nemer. (2017). AutoDock and AutoDockTools for Protein-Ligand Docking: Beta-Site Amyloid Precursor Protein Cleaving Enzyme 1(BACE1) as a Case Study, *Methods Mol. Biol.* 1598, 391-403.
27. R.A. Laskowski, M.B. Swindells. (2011). LigPlot+: multiple ligand-protein interaction diagrams for drug discovery, *J. Chem. Inf. Model.* 51(10), 2778-86.
28. T. James, M.L. Hsieh, L. Knipling, D. Hinton. (2015). Determining the Architecture of a Protein-DNA Complex by Combining FeBABE Cleavage Analyses, 3-D Printed Structures, and the ICM Molsoft Program, *Methods Mol Biol* 1334, 29-40.
29. A. Masunov. (2001). ACD/I-Lab 4.5: an internet service review, *J Chem Inf Comput Sci* 41(4), 1093-5.
30. D. Lagorce, O. Sperandio, J.B. Baell, M.A. Miteva, B.O. Villoutreix. (2015). FAF-Drugs3: a web server for compound property calculation and chemical library design, *Nucleic Acids Res* 43(W1), W200-7.
31. H. Omar, N.M. Hashim, A. Zajmi, N. Nordin, S.I. Abdelwahab, A.H.S. Azizan, A.H.A. Hadi, H.M. Ali. (2013). Aporphine alkaloids from the leaves of Phoebe grandis (Nees) Mer.(Lauraceae) and their cytotoxic and antibacterial activities, *Molecules* 18(8), 8994-9009.
32. A. Urzúa, M. Shamma. (1988). The 4-aryltetralones of Aristolochia chilensis, *Journal of Natural Products* 51(1), 117-121.
33. G.B. Messiano, E.K. Wijeratne, L.M. Lopes, A.L.J.J.o.n.p. Gunatilaka. (2010). Microbial transformations of aryltetralone and aryltetralin lignans by Cunninghamella echinulata and Beauveria bassiana, 73(11), 1933-1937.
34. M.D. Pereira, M.R. Ferreira, G.B. Messiano, I.P. Cerávolo, L.M. Lopes, A.U. Krettli. (2015). Aryltetralols from Holostylis reniformis and syntheses of lignan analogous, *Phytochemistry Letters* 13, 200-205.
35. D. Arbain, M.V. Sargent. (1987). A Preliminary Investigation of The Alkaloid of Phoebe Lanceolata, *ASEAN Journal on Science Technology for Development* 4(1), 41-44.
36. C.A. Lipinski. (2003). Chris Lipinski discusses life and chemistry after the Rule of Five, *Drug Discov. Today* 8(1), 12-6.
37. H.H. Nguyen, M.B. Kim, R.J. Wilson, C.J. Butch, K.M. Kuo, E.J. Miller, Y.A. Tahirovic, E. Jecs, V.M. Truax, T. Wang, C.S. Sum, M.E. Cvijic, G.M. Schroeder, L.J. Wilson, D.C. Liotta. (2018). Design, Synthesis, and Pharmacological Evaluation of Second-Generation Tetrahydroisoquinoline-Based CXCR4 Antagonists with Favorable ADME Properties, *J Med Chem* 61(16), 7168-7188.
38. G. Bocci, E. Carosati, P. Vayer, A. Arrault, S. Lozano, G. Cruciani. (2017). ADME-Space: a new tool for medicinal chemists to explore ADME properties, *Sci Rep* 7(1), 6359.
39. L. Zhu, J. Zhao, Y. Zhang, W. Zhou, L. Yin, Y. Wang, Y. Fan, Y. Chen, H. Liu. (2018). ADME properties evaluation in drug discovery: in silico prediction of blood-brain partitioning, *Mol Divers* 22(4), 979-990.
40. H. Pham-The, M.A. Cabrera-Perez, N.H. Nam, J.A. Castillo-Garit, B. Rasulev, H. Le-Thi-Thu, G.M. Casanola-Martin. (2018). In Silico Assessment of ADME Properties: Advances in Caco-2 Cell Monolayer Permeability Modeling, *Curr Top Med Chem* 18(26), 2209-2229.
41. X. Zhang, T. Liu, X. Fan, N. Ai. (2017). In silico modeling on ADME properties of natural products: Classification models for blood-brain barrier permeability, its application to traditional Chinese medicine and in vitro experimental validation, *J Mol Graph Model* 75, 347-354.
42. J. Wenzel, H. Matter, F. Schmidt. (2019). Predictive Multitask Deep Neural Network Models for ADME-Tox Properties: Learning from Large Datasets, *J Chem Inf Model*.
43. M. Athar Abbasi, H. Raza, R. Aziz Ur, S. Zahra Siddiqui, S. Adnan Ali Shah, M. Hassan, S.Y. Seo. (2018). Synthesis of novel N-(1,3-thiazol-2-yl)benzamide clubbed oxadiazole scaffolds: Urease inhibition, Lipinski rule and molecular docking analyses, *Bioorg Chem* 83, 63-75.
44. C.A. Lipinski, F. Lombardo, B.W. Dominy, P.J.J.A.d.d.r. Feeney. (1997). Experimental and computational approaches to estimate solubility and permeability in drug discovery and development settings, 23(1-3), 3-25.
45. N. Artanti, Y. Ma'arifa, M. Hanafi. (2006). Isolation and identification of active antioxidant compound from Star fruit (Averrhoa carambola) Mistletoe (Dendrophthoe pentandra L.) Miq. ethanol extract, *J Appl Sci* 6, 1659-63.
46. M. Saleem, H.J. Kim, M.S. Ali, Y.S.J.N.P.R. Lee. (2005). An update on bioactive plant lignans, 22(6), 696-716.
47. K.B. Pandey, S.I.J.O.m. Rizvi, c. longevity. (2009). Plant polyphenols as dietary antioxidants in human health and disease, 2(5), 270-278.
48. S. Karkola, K.J.M. Wähälä, c. endocrinology. (2009). The binding of lignans, flavonoids and coumestrol to CYP450 aromatase: a molecular modelling study, 301(1-2), 235-244.